Supplementary Information

Contents:

Whatman, 0.45 μm pore size), all the components were bound together using plastic fastener. b) the lateral view and elevation view of HR-Peeper.

Figure S5. Vertical distribution of labile NO_2^--N in sediment profiles of 18 sampling sites in Lake Taihu, China. The dotted lines at the depth of zero show the position of the SWI.

Figure S6. Dissolved oxygen concentration variation of sediment profile during ABs decay. The dotted lines at the depth of zero show the position of the SWI.

Figure S7. The pH variation of sediment profile during ABs decay. (The computer connected to the microelectrode system failed on day 11 and the data could not be re-determine, resulting in a straight line in the profile). The dotted lines at the depth of zero show the position of the SWI.

Figure S8. The variation of excitation emission matrix fluorescence of the concentration of DOM in the overlying water during ABs decay.

Figure S9. Four unique fluorescent components of DOM in the overlying water during ABs decay.

Figure S10. The maximum fluorescence intensity (F_{max}) of each component during ABs decay.

Figure S11. Vertical distribution of labile NH_4^+-N in sediment profiles during ABs decay. The dotted lines at the depth of zero show the position of the SWI.

Figure S12. Vertical distribution of labile NO_3^--N in sediment profiles during ABs decay. The dotted lines at the depth of zero show the position of the SWI.

Figure S13. Vertical distribution of labile NO_2^--N in sediment profiles during ABs decay. The dotted lines at the depth of zero show the position of the SWI.

Materials and methods

DGT and HR-Peeper deployment and analysis

To ensure the in-situ probes deployment, a newly device was developed. As the Figure S1(A) showed, the device was applied to deploy the sediment probes. The DGT and HR-Peeper probes was fixed in the groove of the plastic disc, to identify the sediment-water interface (Figure S1(B)). The lines and buoys were attached to plastic disc beforehand for the retrieval of the DGT. To calculate the concentrations of DGT-measured, the water temperature was measured by a miniaturized Clark-type microsensor (Unisense, Aarhus, Denmark). The AMP-TH DGT and HR-Peeper devices were carefully vertically inserted into the sediment columns collected from Lake Taihu and retrieved after underwent a diffusive equilibrium period of 24 h and 48 h, respectively. To obtain the masses of target elements in the corresponding resin blanks, 15 standard DGT devices were immersed in the 4 L 0.01 M $NaNO_3$ solutions for 24 h, after which the resin gels were eluted with corresponding extractant. The average masses of NH^{4+}-N, and NO_3^--N in the blank gels were determined as 15.31± 0.21 ng cm^{-2}, and 13.39± 0.11 ng cm^{-2}, respectively. The measurement of detection limit (MDL) was calculated as three times the standard deviation of the blank gels' accumulation mass, which converted to concentrations of 1.13 μg L^{-1}, and 1.01 μg L^{-1}, respectively. These two extracts were used for analysis of labile NH_4^+-N, and NO_3^--N concentrations.

The calculation of DGT concentration

The DGT-labile NH_4^+-N and NO_3^--N concentrations are calculated using equation:

$$C_{DGT} = \frac{M\Delta g}{DAt} \quad [58]$$

The t (s) is the deployment time of DGT. A is the surface area of each gel slice (cm^2). D is the diffusion coefficient of the target elements in the diffusive layer ($cm^2\ s^{-1}$). Δg is the thickness of the diffusive layer (cm). M is the accumulated mass of target elements in the binding gel (mg), which is calculated using equation:

$$M = \frac{C_e V_e}{f_e} \quad [59]$$

Where c_e is the concentration of the target elements in the elution solution (mg L^{-1}), V_e and f_e are the volumes of elution solution (mL) and elution efficiency, respectively.

The apparent flux (F, mg m^{-2} d^{-1}) at the SWI was calculated as follow equation [60,61]:

$$F = F_W + F_S = \left(-D_W \frac{\partial C_w}{\partial X_W}\right)_{x=0} + \left(-\varphi \frac{D_s}{\theta^2} \frac{\partial C_s}{\partial X_S}\right)_{x=0} \quad [38]$$

$$\theta^2 = 1 - \ln(\varphi^2) \quad [60]$$

Where F_W and F_S represent the net diffusive fluxes of target elements DGT-labile concentration of the overlying water and the sediment (mg m^{-2} d^{-1}), respectively; $\frac{\partial C_w}{\partial X_W}$ and $\frac{\partial C_s}{\partial X_S}$ are the DGT-labile concentration gradients (i.e., the slopes) of the overlying water and the sediment, respectively (typically 20 mm or less); C is the concentration of target elements (mg L^{-1}); and x is the depth (cm). D_W and D_S represent the effective diffusion coefficients in water and sediment, respectively; and φ is the porosity in sediment, which was estimated at 0.9 [61]. θ represents the sediment tortuosity (dimensionless).

DNA extraction and quantitative qPCR

Genomic DNA was extracted from the sediment samples using the FastDNA™ Spin Kit for Soil (MP Biomedicals) according to the manufacturer's instructions. The quality and quantity of DNA were checked using agarose gel electrophoresis and by a NanoDrop ND1000 UV/Vis spectral photometer. Extracts were stored at -80°C prior to gene quantification. qPCR was used to quantify functional genes for enzymes of nitrification (AOB *amoA* and AOA *amoA*) and denitrification (*nosZ*). The primers and thermocycling conditions are included in the supplemental information (Table S1). The total qPCR reaction volume of 20 mL contained 10 mL of SYBR green qPCR Master Mix, 1 mL of forward primer, 1 mL of reverse primer, 7 mL of ddH_2O, and 1 mL of the template (DNA). Reactions were performed using an Eco™ Real-Time PCR System. Melting curves were checked for each reaction to confirm the purity of the amplified products. Standard curves were obtained using tenfold serial gradient dilutions of standard plasmids containing targeted genes with known copy numbers. Gene abundance was calculated based on the constructed standard curve, and then converted into copies per gram of dry sediment.

Table S1 Geographic information of the 18 sampling sites in Lake Taihu, China.

Sites	Longitude (E)	Latitude (N)
1	120.0288	31.46674
2	120.0471	31.43271
3	120.0366	31.36847
4	120.1504	31.46746
5	120.1368	31.4389
6	120.1414	31.41028
7	120.2509	31.38162
8	120.2595	31.37974
9	119.9568	31.31049
10	119.9282	31.24647
11	120.095	31.27599
12	120.2887	31.23195
13	120.4125	31.1777
14	120.3349	31.09279
15	120.4313	31.00803
16	120.1529	31.0067
17	120.0519	31.07884
18	120.0114	31.14151

Table S2 The qPCR primers and programs

Target gene	Primer name	Sequence (5'-3')	PCR conditions	Reference
AOB *amoA*	amoA-1F	GGGGTTTCTACTGGTGGT	95°C for 2 min, 35 × [95°C for 15 s, 57°C for 20 s, 72°C for 30 s], 72 °C for 2 min	[32]
	amoA-2R	CCCCTCKGSAAAGCCTTCTTC		
AOA *amoA*	Arch-amoAF	ATGGTCTGGCTWAGACG	95°C for 2 min, 35 × [95°C for 15 s, 57°C for 20 s, 72°C for 30 s], 72°C for 2 min	[32]
	Arch-amoAR	GCCATCCABCKRTANGTCCA		
nosZ	nosZ2F	CGC(A/G)ACGGCAA(G/C)AAGGT(G/C)(A/C)(G/C)(G/C)GT	95°C for 2 min, 35 × [95°C for 15 s, 57°C for 20 s, 72°C for 30 s], 72°C for 2 min	[62]
	nosZ2R	CA(G/T)(A/G)TGCA(G/T)(G/C)GC(A/G)TGGCAGAA		

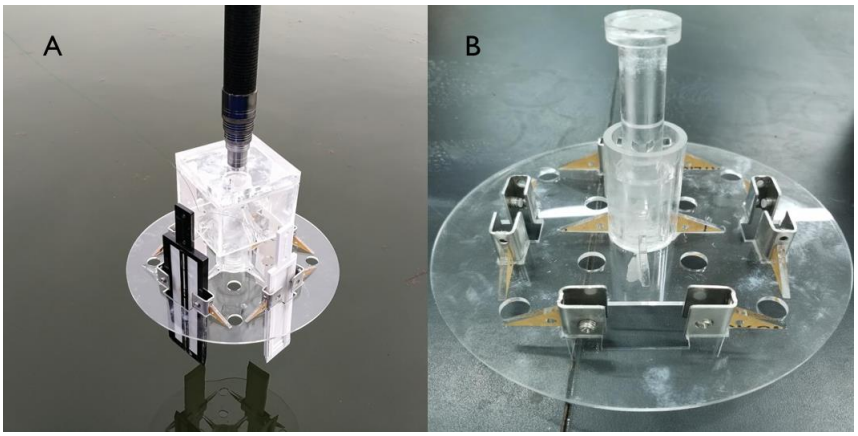

Figure S1. The schematic of DGT deployment device. A) In-situ deployment of DGT and HR-Peeper probes in Lake Taihu; B) Plastic discs for identifying the sediment-water interface.

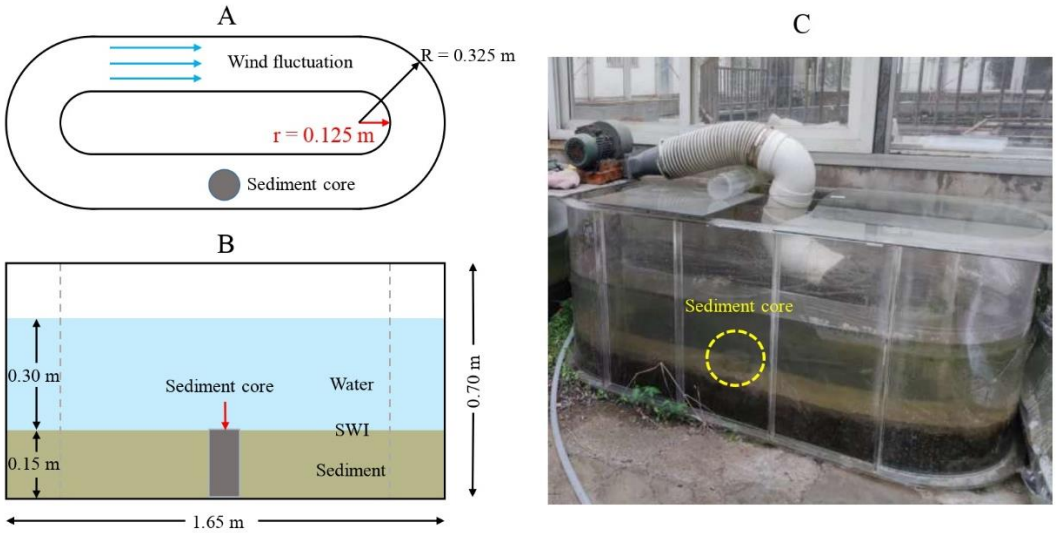

Figure S2. Schematic of the annular flume. A) shows the plan form; B) shows profiles of annular flume; C) is the picture of annular flume. To avoid the excessive crosswise disturbance of the wind, the sediment cores were deployed in the annular flume which on the opposite side of the blower equipment.

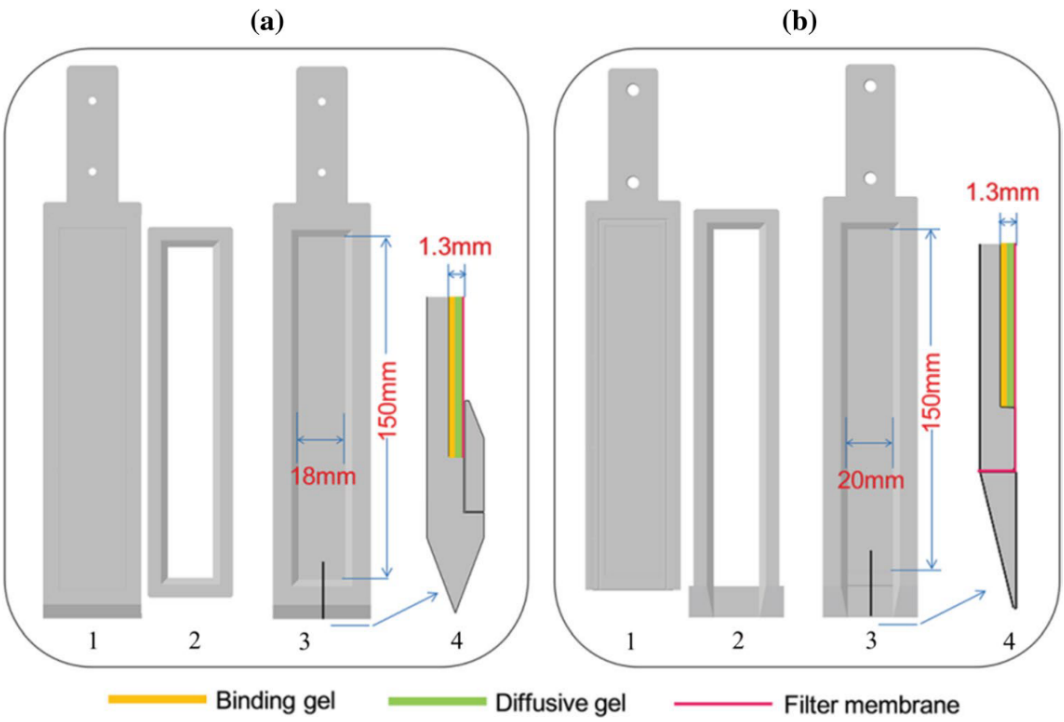

Figure S3. Structure of the traditional flat-type diffusive gradients in thin-film (DGT) device (a) and the new flat-type DGT device (b), the DGT device comprises plastic housing, binding gel, diffusive gel, and filter membrane.

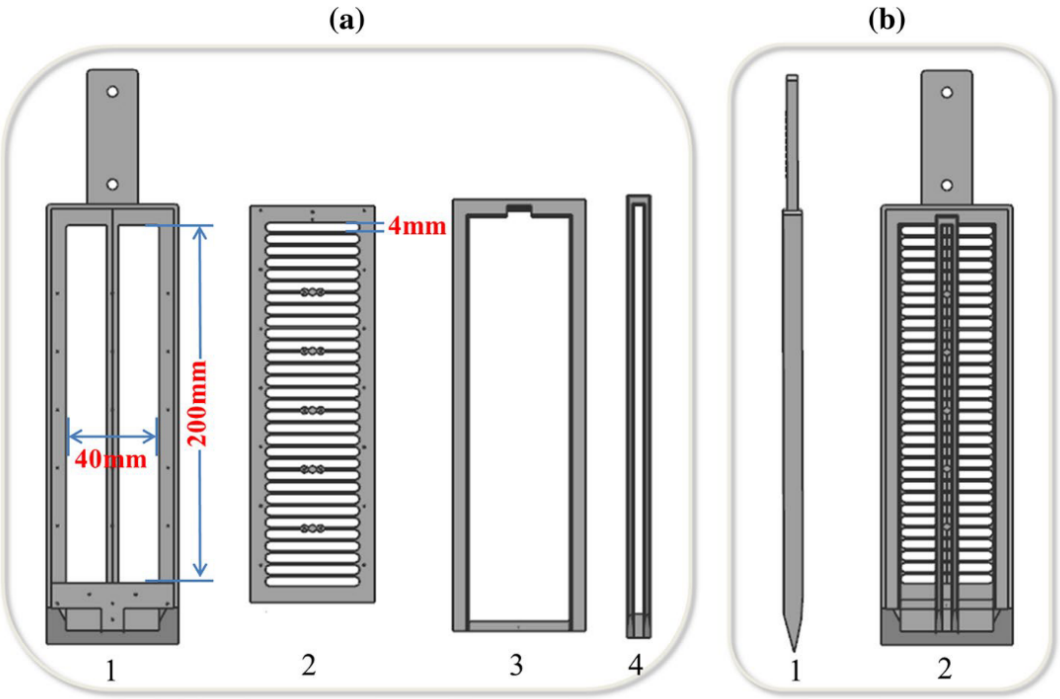

Figure S4. The structure of the HR-Peeper. a). the HR-Peeper was assembled by base plate, plastic window, outer frame and inter frame, in the assembly of the HR-Peeper, the chambers were filled with deionized water and covered with a cellulose nitrate membrane (i.e., dialysis membrane; Whatman, 0.45μm pore size), all the components were bound together using plastic fastener. b). the lateral view and elevation view of HR-Peeper.

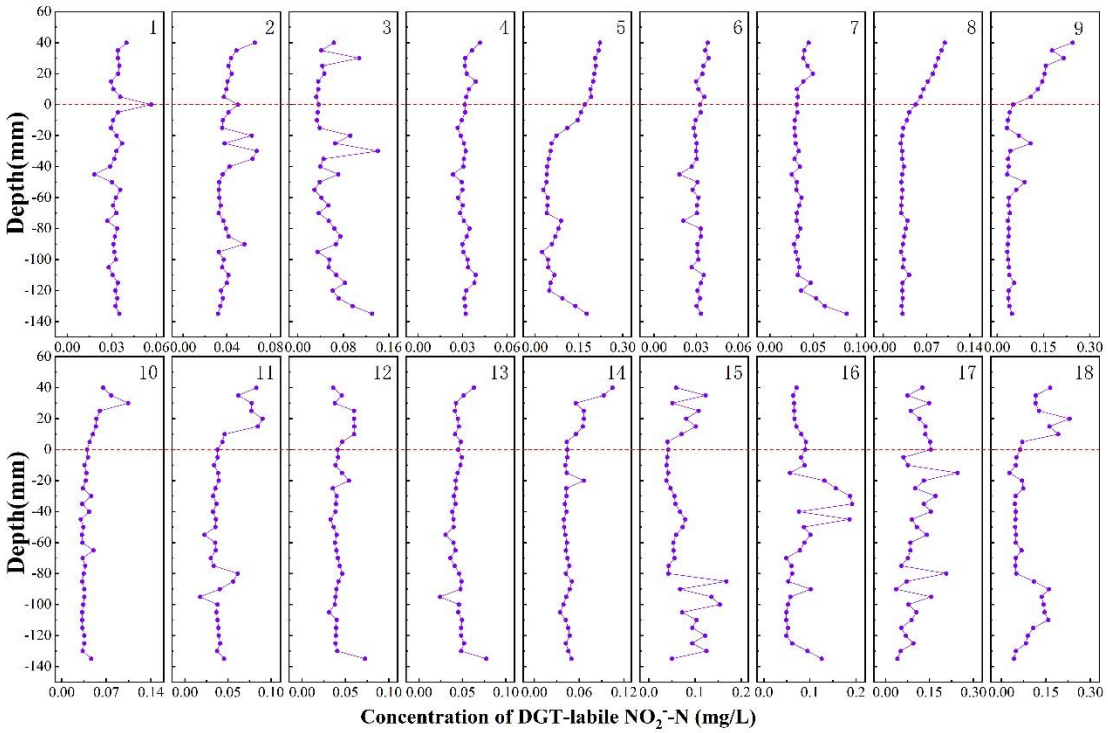

Figure S5. Vertical distribution of labile NO_2^--N in sediment profiles of 18 sampling sites in Lake Taihu, China. The dotted lines at the depth of zero show the position of the SWI.

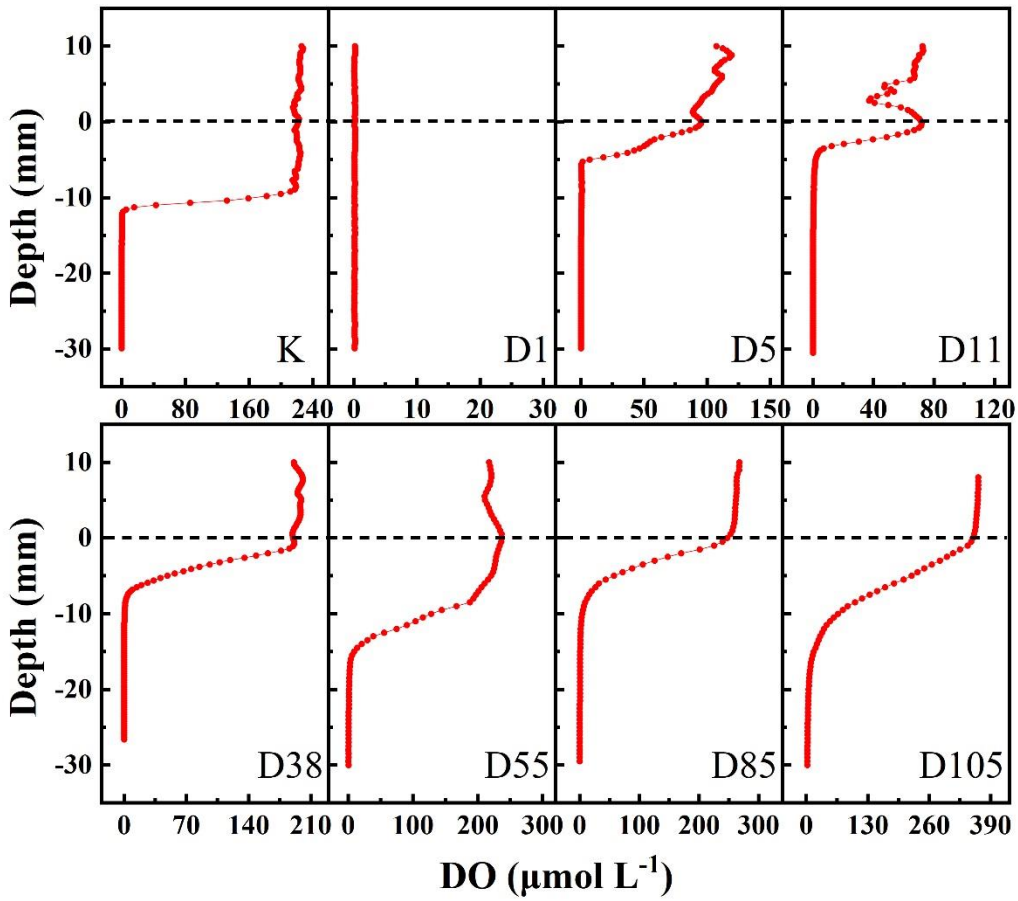

78

79 **Figure S6.** Dissolved oxygen concentration variation of sediment profile during ABs decay. The

80 dotted lines at the depth of zero show the position of the SWI.

81

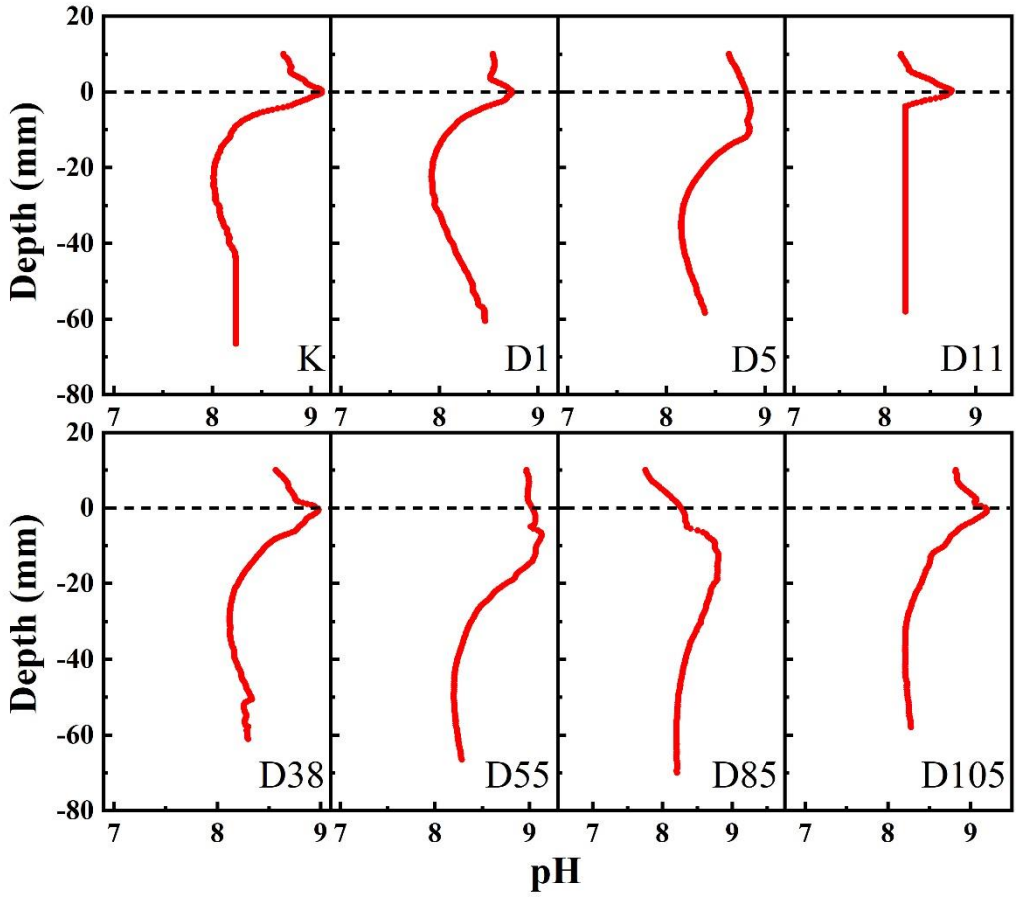

Figure S7. The pH variation of sediment profile during ABs decay. (The computer connected to the microelectrode system failed on day 11 and the data could not be re-determine, resulting in a straight line in the profile). The dotted lines at the depth of zero show the position of the SWI.

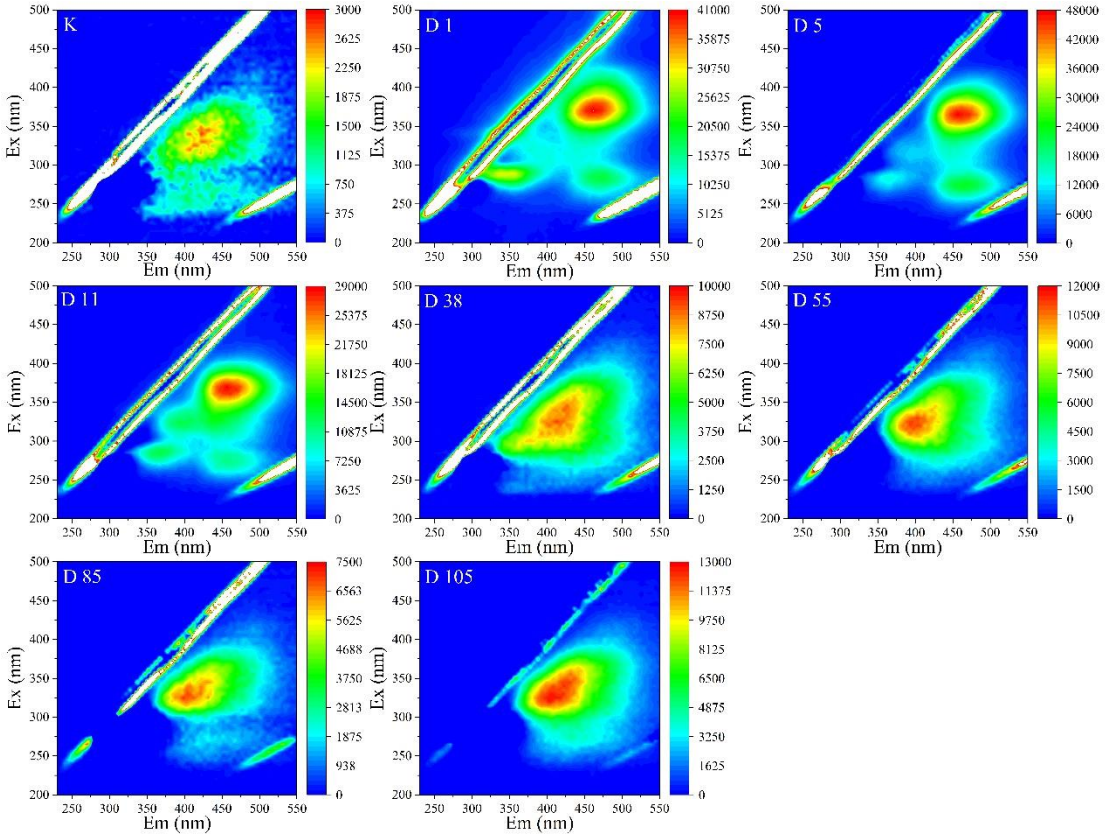

Figure S8. The variation of excitation emission matrix fluorescence of the concentration of DOM in the overlying water during ABs decay.

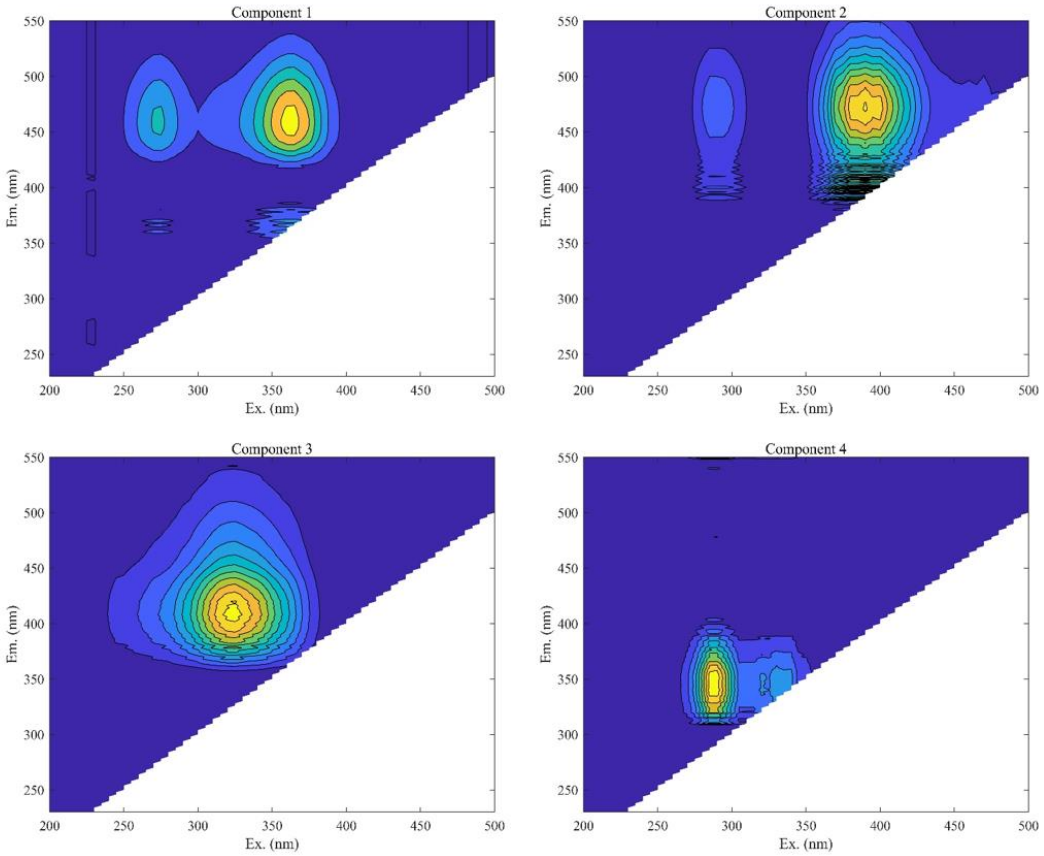

Figure S9. Four unique fluorescent components of DOM in the overlying water during ABs decay.

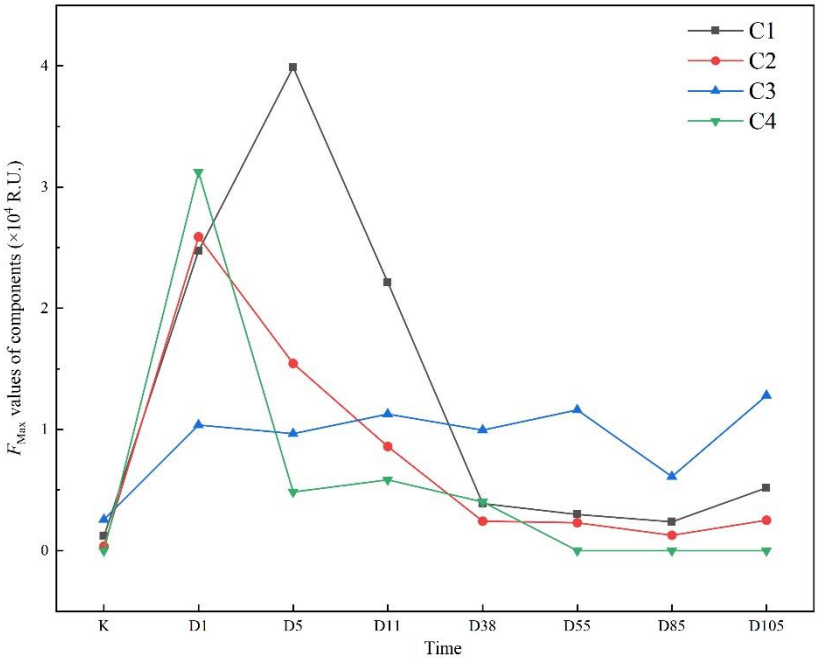

Figure S10. The maximum fluorescence intensity (*F*max) of each component during ABs decay.

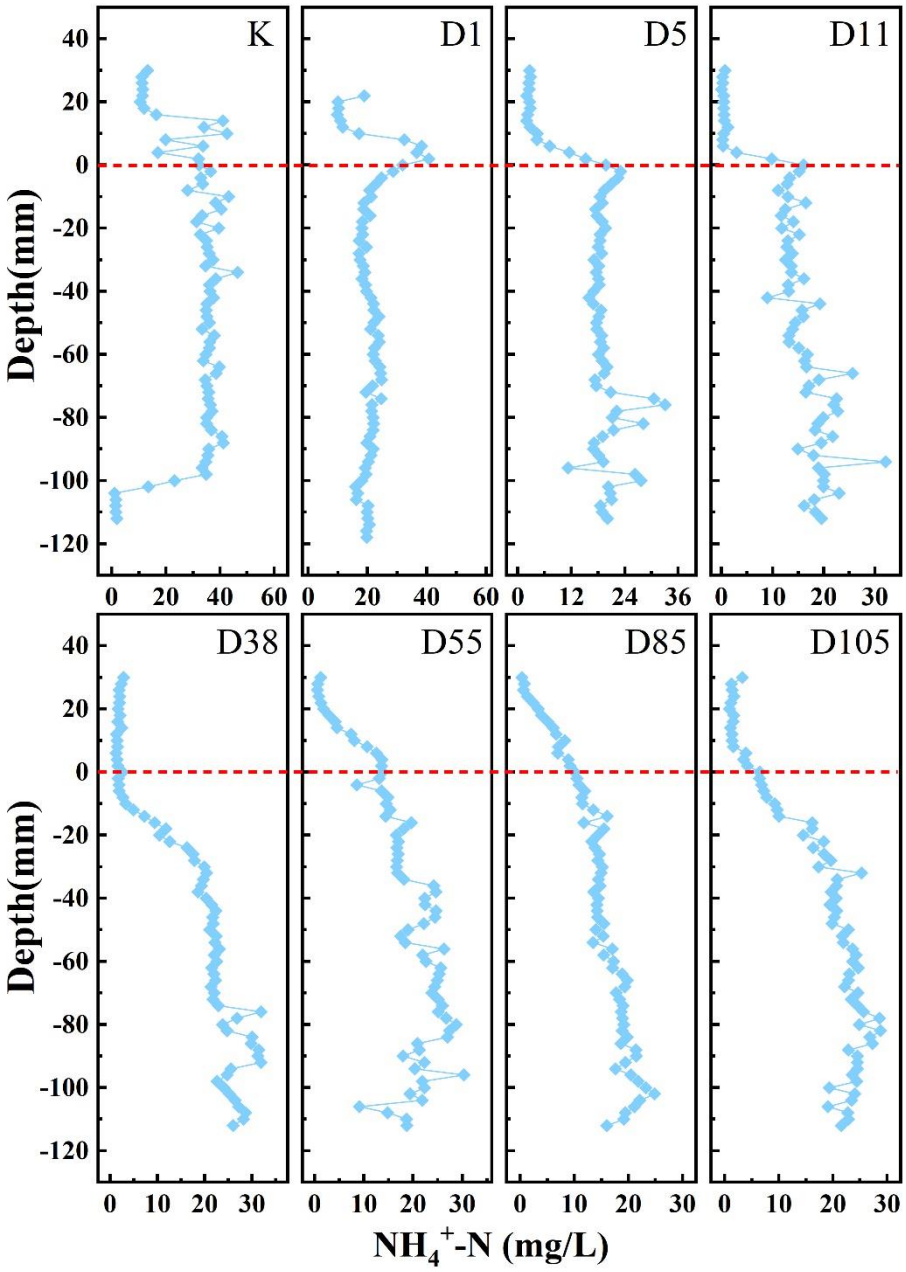

98

99 **Figure S11.** Vertical distribution of labile NH_4^+-N in sediment profiles during ABs decay. The dotted

100 lines at the depth of zero show the position of the SWI.

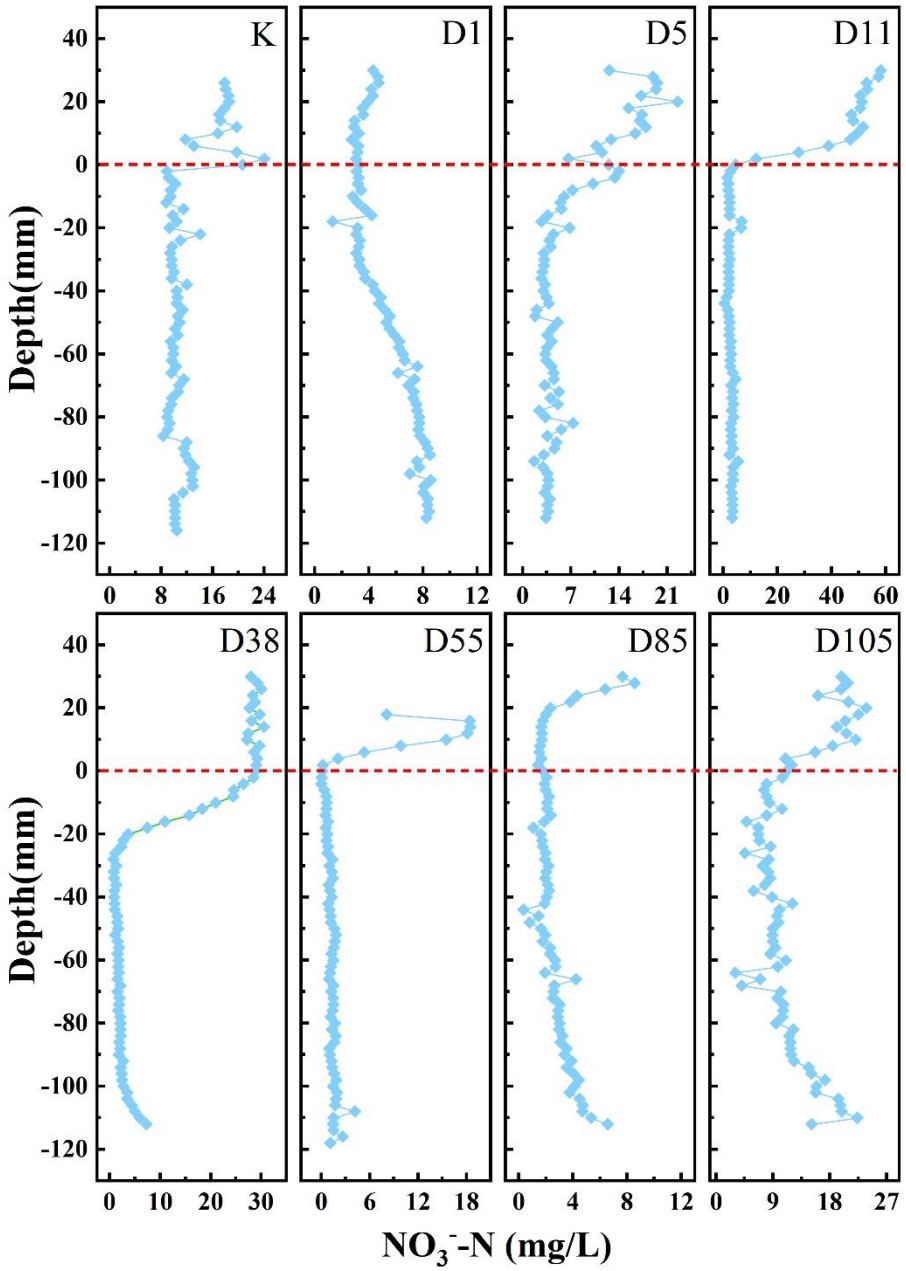

101

102 **Figure S12.** Vertical distribution of labile NO_3^--N in sediment profiles during ABs decay. The dotted

103 lines at the depth of zero show the position of the SWI.

104

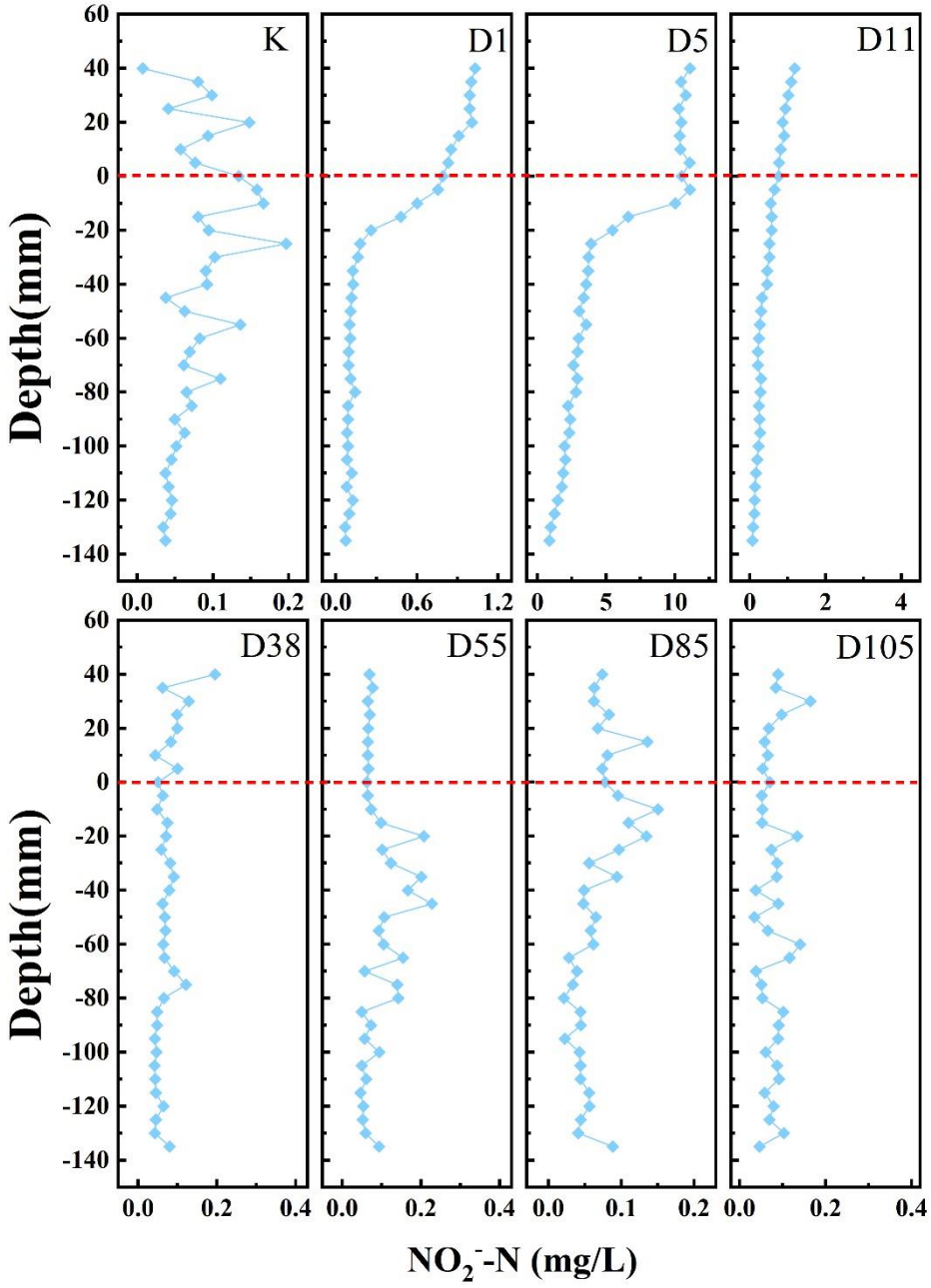

Figure S13. Vertical distribution of labile NO_2^--N in sediment profiles during ABs decay. The dotted lines at the depth of zero show the position of the SWI.